Available online at www.sciencedirect.com
ScienceDirect
Journal of the European Ceramic Society 28 (2008) 2923–2931
www.elsevier.com/locate/jeurceramsoc

Reduced strength degradation of alumina–aluminium titanate composite subjected to low-velocity impact loading

Salvador Bueno [a,b], Lorenzo Micele [a], Carmen Baudin [b], Goffredo de Portu [a,*]

[a] *Institute of Science and Technology for Ceramics (ISTEC), CNR, Via Granarolo 64, 48018 Faenza (RA), Italy*
[b] *Instituto de Cerámica y Vidrio, CSIC, Kelsen 5, 28049 Madrid, Spain*

Received 26 September 2007; received in revised form 10 April 2008; accepted 25 April 2008
Available online 17 June 2008

Abstract

The impact behaviour of monophase alumina and alumina–aluminium titanate monolithic composite ceramics that present flaw tolerant behaviour was studied. Low-velocity impact loading tests were performed on bending bars and the residual strength after the impact was evaluated by four-point bending tests. The impact tests were monitored using an instrumented drop-weight machine. During impact, the composites absorbed higher energy than the monophase material. The strength retention, in percentage, after the impact was significantly higher for the composite that presented damage tolerance for impact energy levels higher than monophase alumina. These results are discussed and fractographic analysis was used to identify the mechanisms responsible for the lower strength degradation of the composite.

Keywords: Al_2O_3; Al_2TiO_5; Composites; Strength; Low-velocity impact

1. Introduction

Ceramic materials are a feasible option in many structural applications due to the technological advantages offered by their hardness, chemical inertness, and high strength-to-weight ratio.[1] However, these applications are limited because of their brittle behaviour and low fracture energy.[2] This implies that severe loading rates, such as those produced during object impact or tool dropping, that could be absorbed easily by metals due to their ductile nature, in the case of ceramics can cause crack initiation, rapid crack propagation, and fracture.[3–6]

The development of impact resistant ceramic materials is still in an early stage of study and associated with the development of structures capable of absorbing a larger amount of energy through damage mechanisms. In particular, to the authors' knowledge, few studies have been performed on the impact behaviour of monolithic fine-grained structural ceramics and most of these dealt with non-oxide materials.[7–16]

The kind and extension of damage mechanisms that take place during the impact determine the impact behaviour.[3,17] However, the damage accumulation in the materials after the impact can lead to a severe loss in the strength and, thus, in the structural integrity necessary for the required applications.[3–4,16,19] The strength of structural ceramics after dynamic loadings, specially in the low-velocity range, can be estimated by the quasi-static theory based on indentation fracture mechanics.[4] Little work has been done in this area, especially under bending testing conditions, and, in general, strength retentions lower than 50% have been reported for different materials after impact conditions leading to barely visible damage.[3–6,11,16]

It is known that the strength of materials showing R-curve behaviour (increasing toughness with crack size) is significantly insensitive to the initial flaw size, i.e. the material exhibits "flaw tolerance".[18,19] Such tolerance would be of great benefit to the structural design of materials subjected to impact because it would reduce the sensitivity to subsequent damage in service and would offer the chance of early detection by non-destructive evaluation.

This "flaw tolerance" approach deals with the development of microstructures that originate toughening mechanisms, most of them caused by localized internal residual stresses in the materials. In particular, alumina (Al_2O_3)–aluminium titanate (Al_2TiO_5) materials can exhibit improved flaw toler-

* Corresponding author.
E-mail address: deportu@istec.cnr.it (G. de Portu).

0955-2219/$ – see front matter © 2008 Elsevier Ltd. All rights reserved.
doi:10.1016/j.jeurceramsoc.2008.04.024

ance and toughness due to thermal expansion mismatch between the two phases. This mismatch induces residual stresses that stimulate microcracking at the grain–matrix interfaces during cooling from the sintering temperature.[20–27] Depending on grain size and grain boundary characteristics, microcracking might also occur during fracture of alumina–aluminium titanate composites.[20,21,28]

In this work, the impact behaviour of a fine-grained monophase alumina and an alumina–aluminium titanate monolithic composite was studied. The latter shows R curve behaviour, with microcracking as the main toughening mechanism.[28] Low-velocity impact loading tests were performed on bending bars and the residual strength retained after the impact was evaluated. The strength retention and the operating reinforcing mechanisms are discussed in terms of the load–velocity relationships recorded during the impact and analyzed by fractographic observations.

2. Impact test parameters

According to the standard equations of dynamics for linear motion of bodies, the parameters that describe the material behaviour submitted to low-velocity impact (velocity of the impactor, $V(t)$; displacement of the impactor, $X(t)$; energy absorbed by the material, $E_a(t)$) can be calculated by integrating the recorded load–time ($P-t$) values during contact and from the velocity at which the impactor hits the specimen (V_0, $t=0$).

When the energy conservation principle is applied to the system (impactor-test sample), the total energy, $E(t)$, is

$$E(t) = E_c(t) + E_p(t) + E_a(t) = \text{const.} \quad (1)$$

where E_c, E_p and E_a refer to kinetic energy, potential energy, and energy absorbed by the sample at time t, respectively. Energy absorption by the impactor is likely to be present, especially when the tested samples are much stiffer than the testing machine. However, because in this study the measurement of the absolute value of the energy is not crucial, the possible energy absorbed by the impact device is not considered when comparing the stiff materials studied. Considering that at $t=0$, just before touching the specimen, the total energy of the impactor $E(0)$ is turned into kinetic energy ($E_c(0)=\text{const.}$), it is possible to determine the energy absorbed by the specimens as a function of the previously quoted parameters, as follows:

$$E_a(t) = E_c(0) - E_c(t) - E_p(t) \quad (2)$$

$$E_a(t) = \frac{m}{2} \times (V_0^2 - V(t)^2) + mgX(t) \quad (3)$$

According to the simple cinematic law, the velocity of a free-fall impactor at $t=0$ (V_0, Eq. (3)) is determined (in the absence of friction) by the drop height (h), by the equation

$$V_0 = \sqrt{2gh} \quad (4)$$

Table 1
Properties of the monolithic materials

	A	A10
ρ (%)	98.1 ± 0.5	97.3 ± 0.5
G_A (μm)	5.5 ± 0.6	3.2 ± 0.4
G_{AT} (μm)	–	2.2 ± 0.1
E (GPa)	388 ± 5	355 ± 4
H_V (GPa)	16.8 ± 1.2	15.6 ± 0.6
K_{IC} (MPa $m^{1/2}$)	3.2 ± 0.1	3.5 ± 0.1
γ_{WOF} (J/m^2)	20 ± 2	33 ± 2

A: monophase alumina; A10: alumina + 10 vol.% aluminium titanate composite. ρ: % of theoretical density; $G_{A,AT}$: grain size of alumina and aluminium titanate grains, respectively; E: dynamic Young's modulus; Hv: Vickers hardness; K_{IC} and γ_{WOF}: fracture toughness and work of fracture.

3. Experimental procedure

3.1. Materials preparation

Monolithic materials of monophase alumina (A) and alumina + aluminium titanate composite with 10 vol.% of second phase (A10, Table 1) were prepared by colloidal filtration from aqueous alumina, Al_2O_3, and titania, TiO_2, suspensions using the optimum green processing conditions already established.[29] Plates measuring 70 mm × 70 mm × 10 mm were obtained by slip casting in plaster moulds, removed from the moulds, and air-dried at room temperature for at least 24 h.

Sintering of the green plates was performed in air in an electrical box furnace (Termiber, Spain). The monophase alumina was sintered at 1550 °C for 3 h, while the alumina + aluminium titanate composite was sintered at 1450 °C for 2 h. All the thermal treatments were performed using heating and cooling rates of 2 °C min^{-1}, with 4 h dwell at 1200 °C during heating.

Densities of the sintered compacts were determined by Archimedes's method in water (European Standard EN 1389:2003) and relative densities were calculated, taking 3.99 g cm^{-3} for alumina (ASTM 42-1468) and 3.70 g cm^{-3} for aluminium titanate (ASTM 26-0040) as theoretical densities. For the composite, a theoretical density value of 3.97 g cm^{-3} was calculated by the rule of mixtures.

The true average grain size was determined by the linear intercept method[30] on microstructural images obtained by field emission gun scanning electron microscope (FEG-SEM, Hitachi, S-4700, Japan) on polished and thermally etched surfaces, considering at least 200 grains for each phase and using the correction factor $4/\pi$.

Young's modulus of the materials was calculated from the resonance frequencies (Grindosonic, J.W. Lemmens, Belgium) of bars (50 mm × 4 mm × 6 mm) tested in flexure by impact and density values. The results reported are the average and the standard deviation of five determinations.

Vickers indentation tests were performed at 50 N (Microtest, Spain), holding the load for 10 s, and the corresponding hardness values were calculated from the applied load and the projected areas of the residual impressions observed by optical microscope (Carl-Zeiss H-P1, Germany).

Fracture toughness and work of fracture were determined by three-point bending tests on Single Edge V Notch Beams (SEVNB) of 50 mm × 4 mm × 6 mm (length by width by thickness) as described elsewhere.[28]

3.2. Impact tests

The impact-testing apparatus used in this study consists of a guided drop-weight test rig instrumented with an impulse data acquisition system (Fig. 1, Instron Dynatup Mini-Tower Model 9200). This machine is capable of performing tests at velocities up to 3.46 m/s (low-velocity range)[3] with a maximum standard drop height, h, of 44 cm. As the drop weight impactor can vary from 1.09 to 4.2 kg, the nominal range of the impact energy ($E = mgh$) is 4.9–18.1 J. The impact tup is hemispherical and has a diameter of 12.7 mm.

The impulse data acquisition system comprises an instrumented type of load cell that digitally records the histories of the impact load–time ($P - t$) at a sampling rate of 1.17 MHz, and a velocity detector block (Fig. 1). The velocity detector records the velocity at which the impactor hits the specimen (V_0, Eqs. (3) and (4)) by using a flag assembled to the falling weight (crosshead) which passes through and interrupts an infrared light beam. Alternatively, it is also possible to insert the theoretical value of V_0 calculated by Eq. (4) in the software. Both operating modes, using the initial velocity determined by the detector block or the initial velocity calculated theoretically were initially investigated. A rebound brake (stop blocks, Fig. 1) is triggered electronically by the velocity detector output, so that the stop blocks move upward, immediately after the tup impacts the specimen, preventing successive impacts.

The specimens were bars measuring 50 mm × 4 mm × 6 mm. A squared support fixture was constructed to hold the samples. The test configuration performed in this study was an impact test with no open window (Fig. 2) in order to induce damage on the impacted surface and to assess the strength degradation after the impact of the samples.

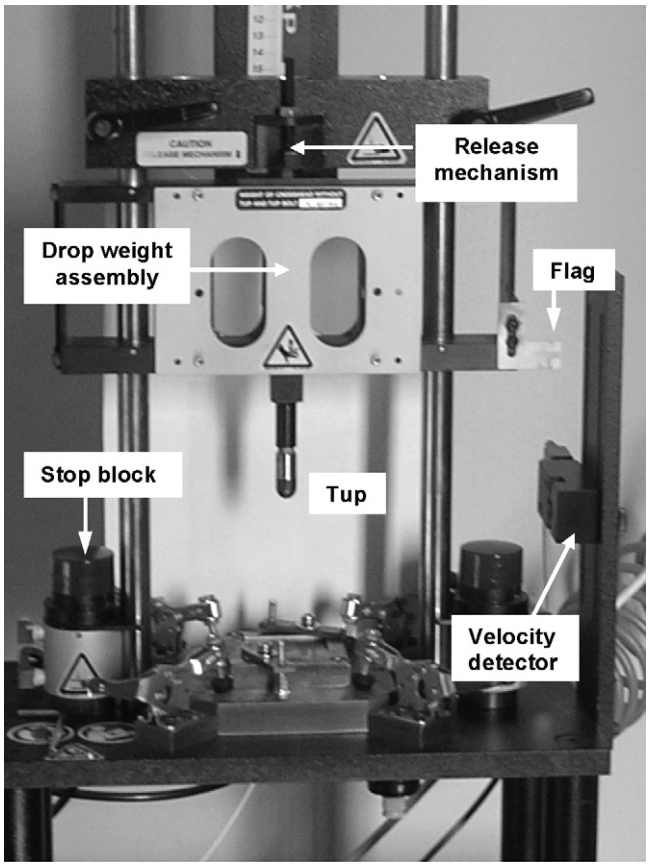

Fig. 1. Photograph of the impact-testing machine used in this study. Tester main components are showed.

The specimens were struck once with a drop weight impactor of 1.09 kg. Different nominal impact energies were used (from $E \cong 0.3$–1.5 J) in order to find an extension of damage adequate to the geometry of the specimens. At least five specimens of each composition were impacted for every nominal energy condition.

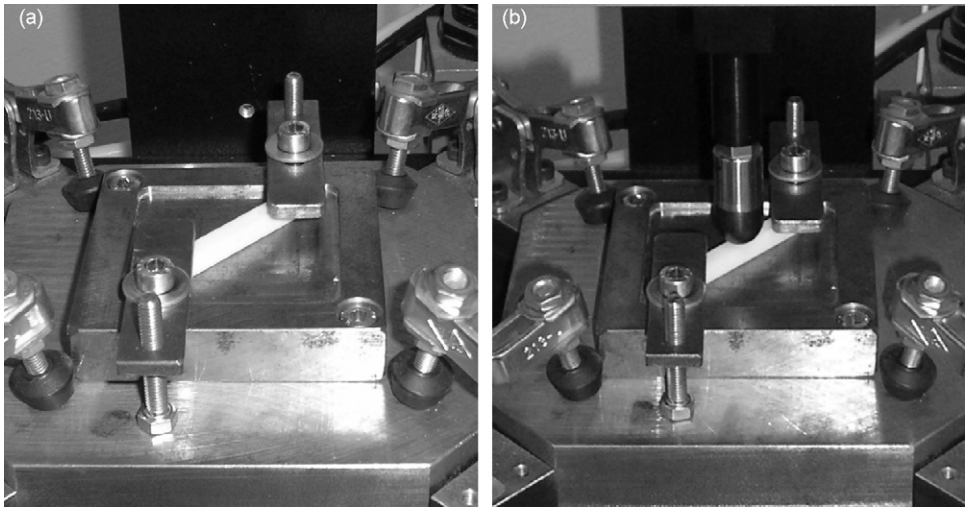

Fig. 2. Detail of the square support fixture assembly of flat edges constructed to hold the samples. The specimens dimensions were bars of 50 mm × 4 mm × 6 mm (a). The tup of the impactor is hemispherical and has a diameter of 12.7 mm (b).

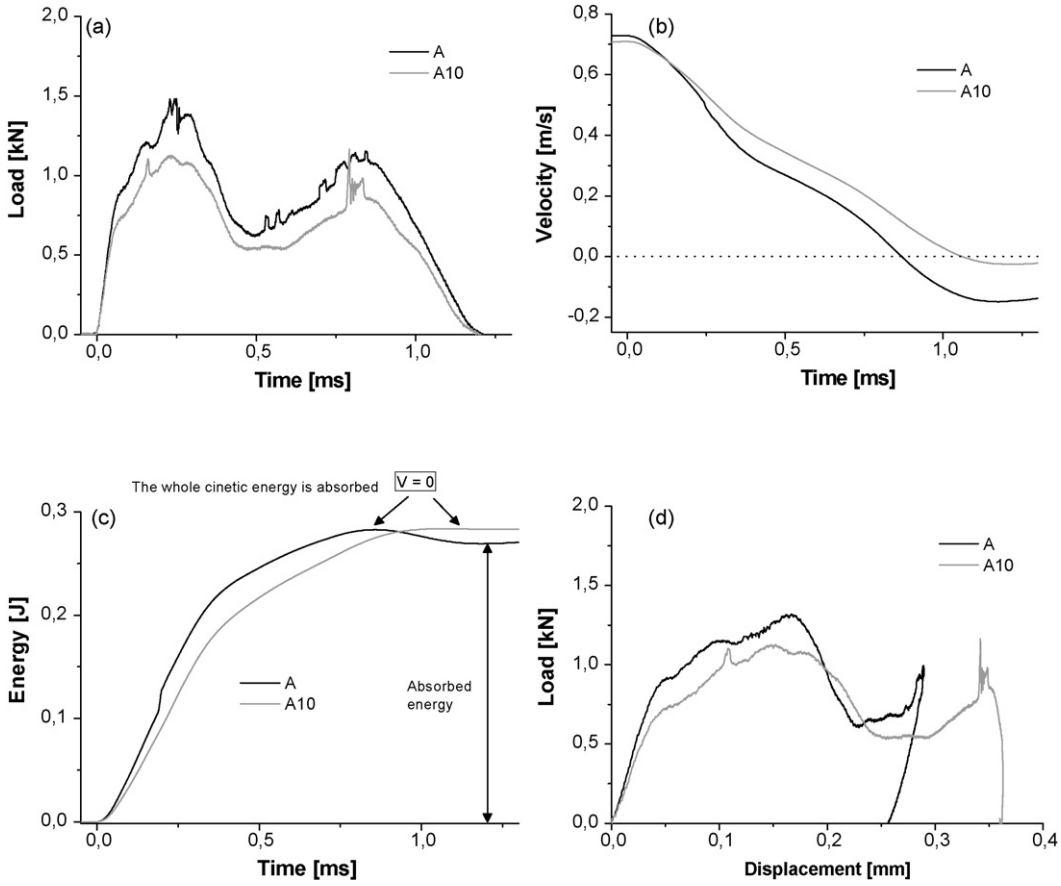

Fig. 3. Characteristic smoothed impact load–time (a), impact velocity–time (b), impact energy–time (c) and load–displacement (d) histories of monolithic specimens during tests performed at 0.3 J.

3.3. Bending strength tests

The bending strength of the materials and the residual strength after the impact were determined by a fully digitalized universal testing machine (Zwick Roell Z050, Germany) using a four-point bending jig with 40 and 20 mm as outer and inner spans, respectively. The cross-head speed was 1 mm min^{-1}. The strength determination of the impacted samples was performed immediately after the impact in order to avoid possible subcritical crack propagation. Given results are the average and the standard deviation of five determinations.

The fracture surfaces of tested specimens were characterized by scanning electron microscopy (SEM Stereoscan 360, UK) and field emission scanning electron microscopy (FE-SEM).

4. Results and discussion

4.1. Impact tests

Due to some experimental critical issues related to the correct position of the velocity detector block and its limited reliability at low velocity, the impact tests on the bending specimens were performed using the theoretical value of the initial impact velocity (V_0, Eq. (4)) corrected for loss due to friction, as will be described below.

The loss of velocity due to friction was estimated by comparison between the theoretically calculated values (V_0, Eq. (4)) and those obtained from the velocity detector block at different nominal impact energies. For tests performed with a nominal impact energy lower than ≅0.5 J (corresponding to an impactor height lower than ≅4–5 cm), it was not possible to find the correct position of the velocity detector block (Fig. 1) due to the limit in the resolution of the system. For tests performed at higher nominal impact energies (0.5–1.5 J), the loss of velocity due to friction was estimated about a 20%.

Different nominal impact energies ($E \cong 0.3$–1.5 J) were used to test the bending specimens in order to find a sufficiently large damage with an extension in keeping with this geometry. The complete failure of the monophase alumina and the alumina–aluminium titanate composite (A10) took place at nominal impact energy of 1.3 and 1.5 J, respectively, and thus, 1.2 J was selected for comparisons between materials. This value ensures the maximum damage accumulation for the alumina materials without a complete failure during the impact tests and then the maximum impact energy suitable for a comparison between the two materials. It is interesting to note that the impact energy necessary to produce the complete failure of the samples was lower for alumina. The order of magnitude of the nominal impact energy necessary to produce the failure of the materials (1.3 and 1.5 J for alumina and A10, respectively) is

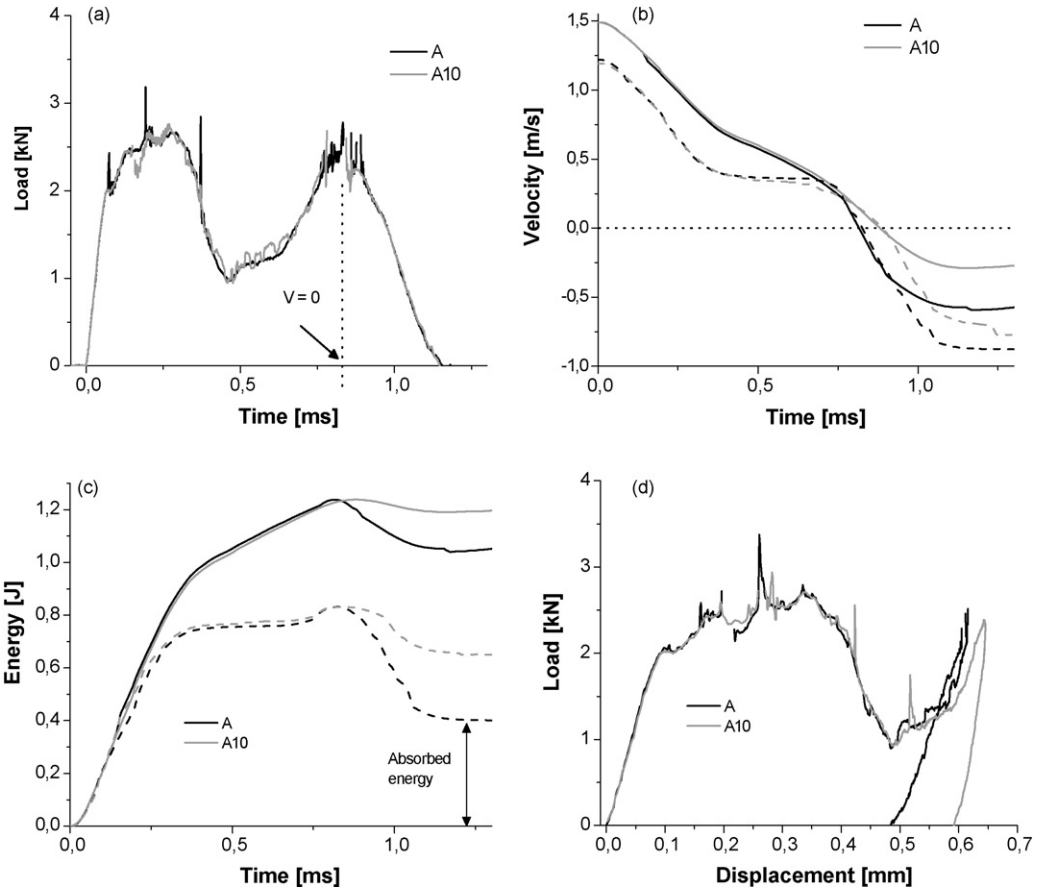

Fig. 4. Characteristic smoothed impact load–time (a), impact velocity–time (b), impact energy–time (c) and load–displacement (d) histories of monolithic specimens during tests performed at 1.2 J. Dashed lines represent velocity and energy calculated from the actual values of initial velocity (V_0) measured by the velocity detector in Fig. 1.

in the range of those reported for strength degradations higher than 50% in bending bars of silicon nitride materials with similar hardness values (14–15 GPa,[6,29] Table 1).

The main features of the impact histories recorded were independent from the particular nominal impact energy. Figs. 3 and 4 show the characteristic curves recorded during impact tests performed with impact energy of 0.3 and 1.2 J, respectively. At the condition established for strength characterization (1.2 J, Fig. 4), most of the specimens supported the impact and provided reliable results, whereas a limited number of them were broken catastrophically during the tests, which could be easily associated to the presence of defects significantly larger than the average ones introduced into the materials during fabrication.

Figs. 3a and 4a present characteristic load–time curves showing two maximum loads recorded at approximately 0.25 and 0.80 ms. The second maximum load could arise as a response to the natural frequency of vibration of the materials that present a cycle period, T, of approximately 0.40 ms, and that can be partially reflected from the interface specimen-support.

For the alumina specimens (A), the reduction of the impactor velocity (Figs. 3b and 4b) occurred faster than for A10 composite specimens. In the case of monophase alumina material, the velocity of the tup was reduced to zero in correspondence of the second maximum load during the impact ($t \cong 0.80$ ms, see Figs. 3a and 4a). In Fig. 4b, the velocity values (solid lines) calculated from the initial theoretical value (V_0, Eq. (4)) are compared to those obtained when V_0 is recorded by the velocity detector (dashed lines, Fig. 4b). The actual value of initial velocity is 20% lower than those calculated theoretically due to friction of the drop weight (crosshead, Fig. 1) along the guided rig. For this reason the theoretical values used for the calculations were reduced by 20%.

In Figs. 3c and 4c, the absorbed energy–time history of the materials is shown. As marked by the arrows in Fig. 3c, when the tup is stopped ($V = 0$), all the energy provided ($\cong 0.3$ J) is absorbed. The total energy absorbed by the specimens was calculated at $t = 1.20$ ms (arrow on the y-axis in Figs. 3c and 4c), when the load applied to the tup is zero (see Figs. 3a and 4a). Alumina–aluminium titanate composites absorbed slightly higher energy than monophase alumina materials. Dashed lines in Fig. 4c correspond, as already described for Fig. 4b, to the absorbed energy calculated from the experimental values of velocity.

To investigate the energy consumption of the specimens in more detail, the impact load–displacement behaviour of the tup and the corresponding area under the curves are shown in Figs. 3d and 4d. During unloading of monophase alumina specimens after the second maximum load, the tup displace-

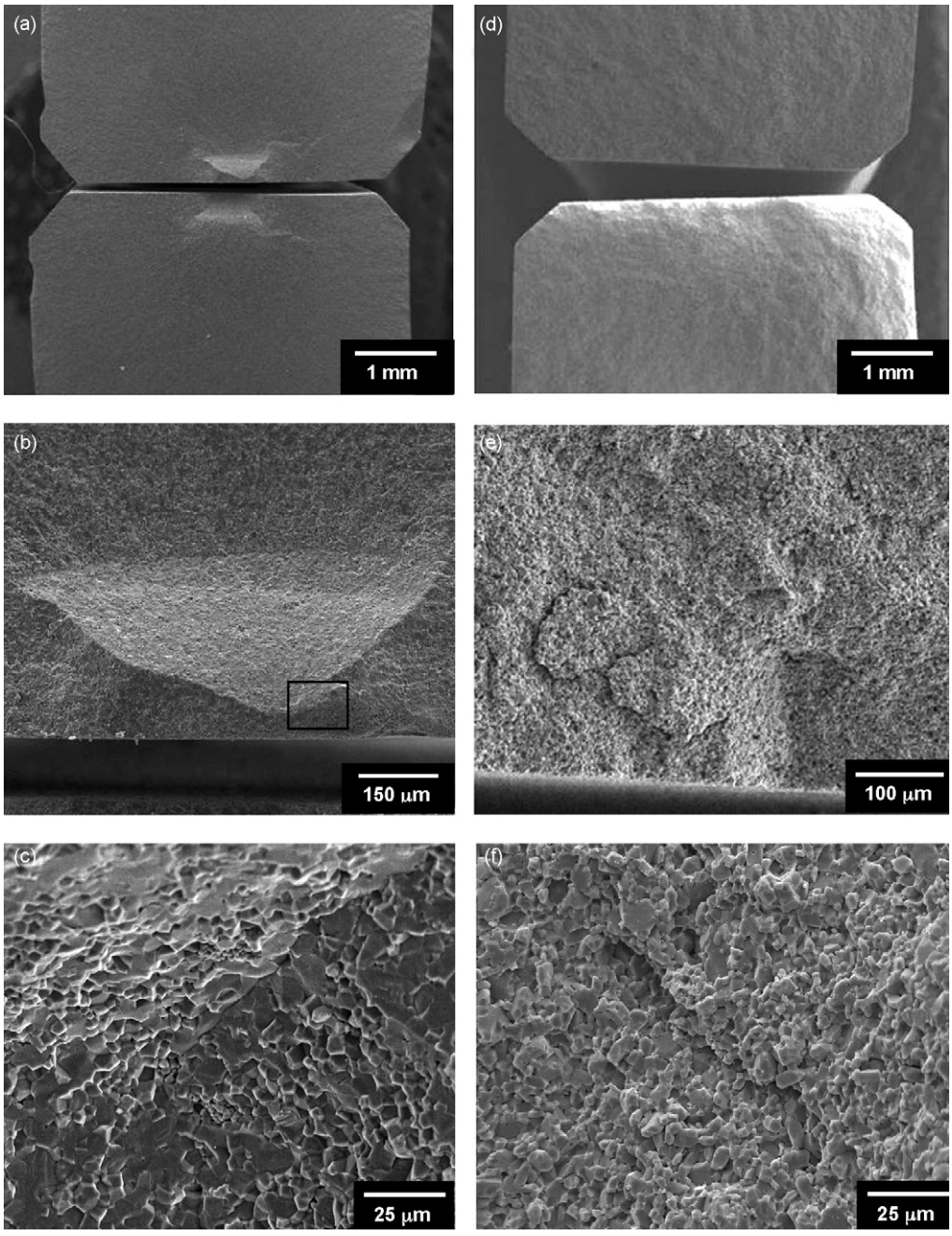

Fig. 5. Characteristic fracture surface of monophase alumina (a–c) and A10 specimen (d–f) impacted at 1.2 J and tested by four-point bending for residual strength characterization. (a) General view of the alumina specimen. A cone crack developed from the impacted face. (b) Detail of the impact point showing the cone crack. (c) Detail of box in (b) revealing mixed trans/intergranular fracture. (d) General view of the A10 composite. No macroscopic features under the impact point were found. (e) Detail showing cracks under the impact point. (f) Detail of a characteristic crack in (e) revealing mostly intergranular fracture.

ment decreased, indicating a more elastic behaviour than that of the composite. In addition, A10 composite specimens showed a larger area under the curve than the monophase alumina, which confirms a larger energy absorption in the composites.

The absence of complete elastic hysteresis for all the materials in the load–displacement curves (Figs. 3d and 4d) and the relatively small values of the returned energy after the impact (difference between nominal impact energy and absorbed energy in Figs. 3c and 4c) are due to the damage accumulation that arose in the materials. The energy absorbed by the specimens when the loss of contact between the tup and the samples takes place has several components: kinetic, elastic, and absorbed due to damage. In stiff materials it is commonly assumed that the first two energies are much lower than the third one, so the total absorbed energy practically coincides with the energy dissipated by damage.[31] However, the small amount of returned energy showed at the lower nominal impact energy condition (0.3 J, Fig. 3c), for which extensive damage accumulation in the materials would not occur, could also be related to some energy absorbed by the impact machine. Nevertheless this

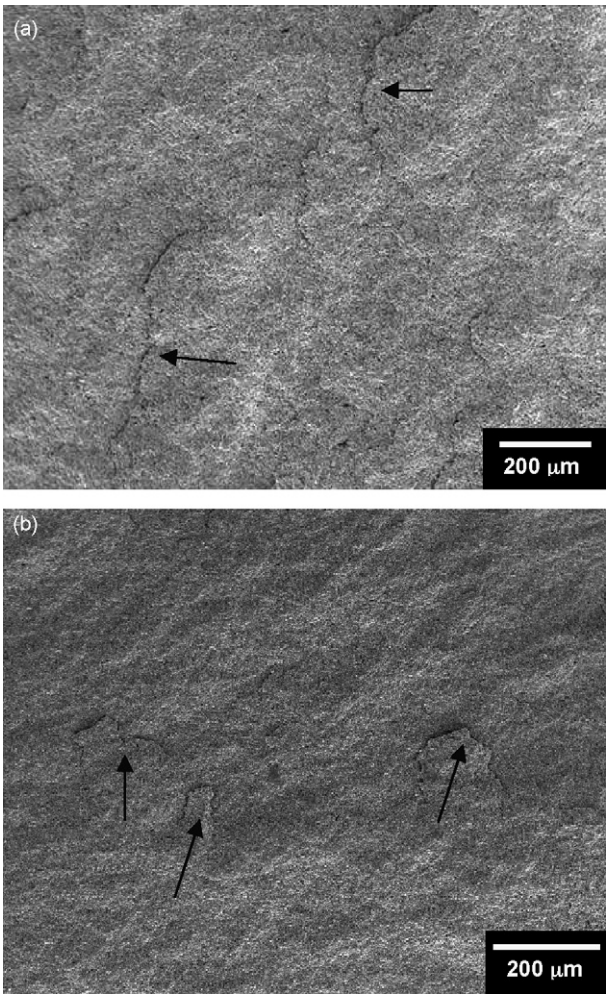

Fig. 6. Comparison of characteristic fracture surfaces of impacted (a) and non-impacted (b) A10 specimens tested by four-point bending, showing cracks (arrows) at ≅1 mm far from the tensile face. Fracture propagates from the bottom part of the image.

systematic error would not influence the relative measurements for comparative purposes between both materials.

Results shown in Figs. 3 and 4 agree with the higher nominal impact energy to failure reported above for the alumina–aluminium titanate composite (1.5 J) when compared with the monophase alumina material (1.3 J). Microscopic observations on fracture surfaces of samples broken for the flexural strength measurements (Figs. 5 and 6) confirm that the higher energy absorbed by the composite is in agreement with a different mode of damage exhibited by the two materials. A detailed discussion of this point is reported in the following paragraph.

4.2. Residual strength

The main microstructural and mechanical properties of the studied monolithic materials are summarized in Table 1 while the bending strength values before and after the impact are showed in Table 2. The non-impacted A10 composite presents lower strength (62%) than monophase alumina in spite of higher fracture toughness and work of fracture values (K_{IC}, γ_{WOF}, Table 1)

Table 2
Strength values of the studied monolithic materials before and after impact test at 1.2 J

	A	A10
σ_f (MPa)	350 ± 32	218 ± 7
$\sigma_{f\,Impacted}$ (MPa)	190 ± 24	167 ± 13
$\sigma_{f\,Retention}$ (%) (min–max)	54 (43–67)	77 (68–85)

Relative mean strength retention is also showed. The lowest and the highest relative strength are reported in parenthesis.

as usually observed for flaw tolerant (R-curve behaviour) materials that failed from natural defects.[32] As described elsewhere,[28] the main toughening mechanism identified in the composite was the development of microcracks during loading of the materials.

After the impact at 1.2 J, barely visible damage without cracking was observed on the surface of samples of both materials. However the residual strength values of both monolithic materials (A and A10, Table 2) were lower. Nevertheless the strength degradation of monophase alumina was more pronounced than that of the composite. In fact, after the impact the differences in flexural strength between the two materials were reduced when compared to the initial strength (A10 composites exhibited 88% of the alumina strength compared to 62% before the impact). This means that the composite, due to its higher flaw tolerance, presents a significantly larger strength retention (77% of the original one instead of 54% for monophase alumina, Table 2).

Fractographic observations in Fig. 5 revealed the different fracture modes of the impacted alumina and alumina–aluminium titanate specimens. Alumina specimens (Fig. 5a–c) showed characteristic cone-cracks similar to those described for brittle materials under Hertzian contact[33] or spherical impact loadings.[4,6,16] These cone-cracks are developed under the impact point and give rise to the lower strength retention (Table 2) of these materials. The fracture across the whole fracture surface, i.e. cone crack and subsequent propagation during the bending tests, was mixed transgranular/intergranular (Fig. 5c) as observed on fracture surface of non-impacted alumina specimens as well as on other aluminas with similar grain size.[34]

Conversely, A10 composites (Fig. 5d) did not show any macroscopic feature at the impact point. At larger magnifications, diffuse damage zones constituted by cracks in the range of 100–400 μm (Fig. 5e) and mostly intergranular fracture (Fig. 5f) were observed on the fracture surfaces both close to the impacted surfaces and in the bulk of the specimens.

Non-impacted A10 samples also presented mostly intergranular fracture and microcracks across the fracture surfaces (Fig. 6a). Nevertheless, the comparison between the fracture surfaces of impacted and non-impacted A10 samples (Fig. 6) revealed that the sizes of the microcracks were larger in the former (crack lengths up to 400 μm, Fig. 6a) than in the non-impacted ones (crack lengths ≅150 μm). This demonstrates that a diffuse damage zone was formed in the A10 composites during impact. The formation of this zone impeded the formation of a localized damaged zone like the one that developed in monophase alumina (cone crack, Fig. 5), and gave rise to higher strength retention and absorbed energy during the impact.

The formation of diffuse damage in the alumina–aluminium titanate composites under impact conditions is similar to that previously observed for specimens indented with a Vickers pyramid,[35] and in materials with heterogeneous microstructures, like those described by Lawn et al.[36–38], under Hertzian contact tests. These heterogeneous materials show the capability for dispersing potentially dangerous surface cracks due to the generation of a diffuse shear-fault damage zone and are traditionally located as internal layers of laminated structures. In this way, the heterogeneous layer inhibits the development of cone cracking in the homogeneous brittle outer layers.

The homogeneous fine-grained alumina–aluminium titanate composite presented in this work as a monolithic structure showed relatively low strength degradation (≅20%, Table 2) even after impact conditions (1.2 J) close to those necessary to produce the catastrophic failure of the specimens (1.3–1.5 J for the monophase alumina and the A10 composite, respectively).

5. Concluding remarks

The results of some preliminary experiments exploring the impact resistance of a monolithic fine-grained alumina and an alumina–aluminium titanate ceramic composite are presented. The composite, even if an isotropic monolithic structure, shows lower strength degradation after impact than that of monolithic monophase alumina. This behaviour can be attributed to the development of a diffuse microcracked damage zone that acts as an energy dissipation mechanism. The composite supported higher impact energies than monophase alumina prior to complete failure of the specimens. In addition the strength retention of the composite (77% of the original one) was higher than that exhibited by monophase alumina (54%) for an impact energy close to those producing the catastrophic failure of the specimens.

Acknowledgments

The authors would like to acknowledge the support of the Project MEC MAT2006-13480 C02-01, the Postdoctoral Fellowship (S. Bueno) MEC EX-2006-0555 (Spain) and the Italian Regional Project MATMEC.

References

1. Brook, R. J., Advanced ceramic materials: An overview. In *Concise Encyclopedia of Advanced Ceramic Materials*, ed. R. J. Brook, R. W. Cahn and M. B. Bever. Pergamon Press, Oxford, 1991, pp. 1–8.
2. Davidge, R. W., The fracture strength of ceramics. In *Mechanical Behaviour of Ceramics*, ed. R. W. Cahn, M. W. Thompson and I. M. Ward. Cambridge University Press, Cambridge, 1979, pp. 75–103.
3. Richardson, M. O. W. and Wisheart, M. J., Review of low-velocity impact properties of composite materials. *Compos. A*, 1996, **27A**, 1123–1131.
4. Wiederhorn, S. M. and Lawn, B. R., Strength degradation of glass resulting from impact with spheres. *J. Am. Ceram. Soc.*, 1977, **60**, 451–458.
5. Oh, S. Y., Shin, H. S. and Suh, C. M., Evaluation of biaxial bending strength in damaged soda-lime glass. *Int. J. Mod. Phys. B*, 2003, **17**, 1329–1334.
6. Choi, S. R., Pereira, J. M., Janosik, L. A. and Bhatt, R. T., Foreign object damage in flexure bars of two gas-turbine grade silicon nitrides. *Mater. Sci. Eng. A.—Struct. Mater. Prop. Microstruct. Process*, 2004, **379**, 411–419.
7. Kennedy, G., Ferranti, L., Russell, R., Zhou, M. and Thadhani, N., Dynamic high-strain-rate mechanical behavior of microstructurally biased two-phase $TiB_2 + Al_2O_3$ ceramics. *J. Appl. Phys.*, 2002, **91**, 1921–1927.
8. Staehler, J. M., Predebon, W. W., Pletka, B. J. and Subhash, G., Micromechanisms of deformation in high-purity hot-pressed alumina. *Mater. Sci. Eng. A—Struct. Mater. Prop. Microstruct. Process*, 2000, **291**, 37–45.
9. Normandia, M. J., Impact response and analysis of several silicon carbides. *Int. J. Appl. Ceram. Technol.*, 2004, **1**, 226–234.
10. Bourne, N., Millett, J., Rosenberg, Z. and Murray, N., On the shock induced failure of brittle solids. *J. Mech. Phys. Solids*, 1998, **46**, 1887–1908.
11. Marschall, J., Erlich, D. C., Manning, H., Duppler, W., Ellerby, D. and Gasch, M., Microhardness and high-velocity impact resistance of HfB_2/SiC and ZrB_2/SiC composites. *J. Mater. Sci.*, 2004, **39**, 5959–5968.
12. Luo, H. Y. and Chen, W. N., Dynamic compressive response of intact and damaged AD995 alumina. *Int. J. Appl. Ceram. Technol.*, 2004, **1**, 254–260.
13. Chen, M. W., McCauley, J. W., Dandekar, D. P. and Bourne, N. K., Dynamic plasticity and failure of high-purity alumina under shock loading. *Nat. Mater.*, 2006, **5**, 614–618.
14. Forquin, P., Denoual, C., Cottenot, C. E. and Hild, F., Experiments and modelling of the compressive behaviour of two SiC ceramics. *Mech. Mater.*, 2003, **35**, 987–1002.
15. Wang, H. and Ramesh, K. T., Dynamic strength and fragmentation of hot-pressed silicon carbide under uniaxial compression. *Acta Mater.*, 2004, **52**, 355–367.
16. Akimune, Y., Katano, Y. and Matoba, K., Spherical-impact damage and strength degradation in silicon nitrides for automobile turbocharger rotors. *J. Am. Ceram. Soc.*, 1989, **72**, 1422–1428.
17. Schoeppner, G. A. and Abrate, S., Delamination threshold loads for low velocity impact on composite laminates. *Compos. A*, 2000, **31**, 903–915.
18. Evans, A. G., Perspective on the development of high-toughness ceramics. *J. Am. Ceram. Soc.*, 1990, **73**, 187–206.
19. Bennison, S. J. and Lawn, B. R., Flaw tolerance in ceramics with rising crack-resistance behavior. *J. Mater. Sci.*, 1989, **24**, 3169–3175.
20. Lawn, B. R., Padture, N. P., Braun, L. M. and Bennison, S. J., Model for toughness curves in two-phase ceramics. I. Basic fracture mechanics. *J. Am. Ceram. Soc.*, 1993, **76**, 2235–2240.
21. Padture, N. P., Runyan, J. L., Bennison, S. J., Braun, L. M. and Lawn, B. R., Model for toughness curves in two-phase ceramics. II. Microstructural variables. *J. Am. Ceram. Soc.*, 1993, **76**, 2241–2247.
22. Padture, N. P., Bennison, S. J. and Chan, H. M., Flaw-tolerance and crack-resistance properties of alumina–aluminium titanate composites with tailored microstructures. *J. Am. Ceram. Soc.*, 1993, **76**, 2312–2320.
23. Runyan, J. L. and Bennison, S. J., Fabrication of flaw-tolerant aluminium-titanate-reinforced alumina. *J. Eur. Ceram. Soc.*, 1991, **7**, 93–99.
24. Uribe, R. and Baudin, C., Influence of a dispersion of aluminium titanate particles of controlled size on the thermal shock resistance of alumina. *J. Am. Ceram. Soc.*, 2003, **86**, 846–850.
25. Baudin, C., Sayir, A. and Berger, M. H., Mechanical behaviour of directionally solidified alumina/aluminium titanate ceramics. *Acta Mater.*, 2006, **54**, 3835–3841.
26. Bueno, S. and Baudin, C., Layered materials with high strength and flaw tolerance based on alumina and aluminium titanate. *J. Eur. Ceram. Soc.*, 2007, **27**, 1455–1462.
27. Dakskobler, A. and Kosmac, T., Preparation and properties of aluminium titanate–alumina composites. *J. Mater. Res.*, 2006, **21**, 448–454.
28. Bueno, S., Berger, M. H., Moreno, R. and Baudin, C., Fracture behaviour of microcrack-free alumina–aluminium titanate ceramics with second phase nanoparticles at alumina grain boundaries. *J. Eur. Ceram. Soc.*, 2008, **28**, 1961–1971.
29. Bueno, S., Moreno, R. and Baudin, C., Reaction sintering Al_2O_3/Al_2TiO_5 microcrack-free composites obtained by colloidal filtration. *J. Eur. Ceram. Soc.*, 2004, **24**, 2785–2791.
30. Fullmann, R. L., Measurement of particle sizes in opaque bodies. *Trans. AIME J. Metals*, 1953, **197**, 447.
31. Gómez-del Río, T., Zaera, T., Barbero, E. and Navarro, C., Damage in CFRPs due to low velocity impact on low temperature. *Compos. B*, 2005, **36**, 41–50.
32. Steinbrech, R. W., Toughening mechanisms for ceramic materials. *J. Eur. Ceram. Soc.*, 1992, **10**, 131–142.

33. Lawn, B. R., Wiederhorn, S. M. and Johnson, H. H., Strength degradation of brittle surfaces: blunt indenters. *J. Am. Ceram. Soc.*, 1975, **58**, 428–432.
34. Mussler, B., Swain, M. and Claussen, N., Dependence of fracture toughness of alumina on grain size and test technique. *J. Am. Ceram. Soc.*, 1982, **65**, 566–572.
35. Bueno, S. and Baudin, C., Instrumented Vickers microindentation of alumina based materials. *J. Mater. Res.*, 2006, **21**, 161–173.
36. Wuttiphan, S., Lawn, B. R. and Padture, N. P., Crack suppression in strongly bonded homogeneous/heterogeneous laminates: a study on glass/glass-ceramic bilayers. *J. Am. Ceram. Soc.*, 1996, **79**, 634–640.
37. An, L., Chan, H. M., Padture, N. P. and Lawn, B. R., Damaged resistant alumina-based layer composites. *J. Mater. Res.*, 1996, **11**, 204–210.
38. Liu, H., Lawn, B. R. and Hsu, S. M., Hertzian contact response of tailored silicon nitride multilayers. *J. Am. Ceram. Soc.*, 1996, **79**, 1009–1014.